Universiteit
Leiden
The Netherlands

Chromatin modifiers in DNA repair and human disease

Helfricht, A.

Citation
Helfricht, A. (2016, November 1). *Chromatin modifiers in DNA repair and human disease*. Retrieved from https://hdl.handle.net/1887/43800

Version:	Not Applicable (or Unknown)
License:	Licence agreement concerning inclusion of doctoral thesis in the Institutional Repository of the University of Leiden
Downloaded from:	https://hdl.handle.net/1887/43800

Note: To cite this publication please use the final published version (if applicable).

Cover Page

Universiteit Leiden

The handle http://hdl.handle.net/1887/43800 holds various files of this Leiden University dissertation.

Author: Helfricht, A.
Title: Chromatin modifiers in DNA repair and human disease
Issue Date: 2016-11-01

3

REMODELING AND SPACING FACTOR 1 (RSF1) DEPOSITS CENTROMERE PROTEINS AT DNA DOUBLE-STRAND BREAKS TO PROMOTE NON-HOMOLOGOUS END-JOINING

Angela Helfricht[1], Wouter W. Wiegant[1], Peter E. Thijssen[1,2], Alfred C. Vertegaal[3], Martijn S. Luijsterburg[1] and Haico van Attikum[1]

[1]Department of Toxicogenetics; Leiden University Medical Center
[2]Department of Human Genetics; Leiden University Medical Center
[3]Department of Molecular Cell Biology; Leiden University Medical Center

An adapted version of this manuscript has been published in Cell Cycle 2013 vol 12 (18)

ABSTRACT

The cellular response to ionizing radiation (IR)-induced DNA double-strand breaks (DSBs) in native chromatin requires a tight coordination between the activities of DNA repair machineries and factors that modulate chromatin structure. SMARCA5 is an ATPase of the SNF2 family of chromatin remodeling factors that has recently been implicated in the DSB response. It forms distinct chromatin-remodeling complexes with several non-canonical subunits, including the remodeling and spacing factor 1 (RSF1) protein. Despite the fact that RSF1 is often overexpressed in tumors and linked to tumorigenesis and genome instability, its role in the DSB response remains largely unclear. Here we show that RSF1 accumulates at DSB sites and protects human cells against IR-induced DSBs by promoting repair of these lesions through homologous recombination (HR) and non-homologous end-joining (NHEJ). Although SMARCA5 regulates the RNF168-dependent ubiquitin response that targets BRCA1 to DSBs, we found RSF1 to be dispensable for this process. Conversely, we found that RSF1 facilitates the assembly of centromere proteins CENP-S and CENP-X at sites of DNA damage, while SMARCA5 was not required for these events. Mechanistically, we uncovered that CENP-S and CENP-X, upon their incorporation by RSF1, promote assembly of the NHEJ factor XRCC4 at damaged chromatin. In contrast, CENP-S and CENP-X were dispensable for HR, suggesting that RSF1 regulates HR independently of these centromere proteins. Our findings reveal distinct functions of RSF1 in the two major pathways of DSB repair and explain how RSF1, through the loading of centromere proteins and XRCC4 at DSBs, promotes repair by non-homologous end-joining.

INTRODUCTION

Chromosomal DNA double-strand breaks (DSBs), which can arise after exposure of cells to ionizing radiation (IR) or as a consequence of DNA replication stress, form a major threat to genome stability. Their inefficient or inaccurate repair can result in chromosome rearrangements and translocations, which may result in cancer development or cell death (Jackson and Bartek, 2009). To circumvent the deleterious effects of DSBs, cells activate the DNA damage response (DDR), which comprises events that lead to detection and repair of these lesions, as well as a delay in cell cycle progression (Ciccia and Elledge, 2010; Jackson and Bartek, 2009). DSB repair involves two dedicated pathways known as non-homologous end-joining (NHEJ) and homologous recombination (HR) (Chapman et al., 2012). While NHEJ re-joins the ends of a DSB in an error-free or error-prone manner and is active throughout the cell cycle, HR mediates the error-free repair of DSBs in S or G2 phase by using the sequence information obtained from a homologous template, usually a sister chromatid. DSBs occur in DNA that is tightly packaged into higher-order chromatin fibers. Emerging evidence suggests that DSB repair is closely coordinated with chromatin structure and function. Several proteins involved in modulating chromatin structure, including histone-modifying enzymes and ATP-dependent chromatin remodeling complexes are critically important for DSB repair (Luijsterburg and van, 2011; Smeenk and van, 2013). A key modification that occurs throughout DSB-associated chromatin is the ATM kinase-dependent phosphorylation of histone H2A variant H2AX (γH2AX). This γH2AX histone mark then leads to the recruitment of two distinct ubiquitin E3 ligases, RNF8 and RNF168, which are responsible for the ubiquitylation of damaged chromatin and the subsequent accumulation of BRCA1 through its ubiquitin-binding partner RAP80 (Doil et al., 2009; Huen et al., 2007; Mailand et al., 2007; Stewart et al., 2009; Wang and Elledge, 2007). Interestingly, these histone marks have recently been shown to co-operate with distinct ATP-dependent remodeling factors in orchestrating the DSB response. Specifically, we found that the chromatin remodelers CHD4 and SMARCA5 are recruited to DSBs where they interact with the RNF8 and RNF168 ubiquitin ligases and affect the ubiquitin-dependent signaling of DSBs at the level of RNF8 and RNF168, respectively (Larsen et al., 2010; Luijsterburg et al., 2012a; Smeenk et al., 2010; Smeenk et al., 2013). Consequently, loss of CHD4 or SMARCA5 abrogates BRCA1 accumulation and leads to defects in DSB repair (Lan et al., 2010; Larsen et al., 2010; Luijsterburg et al., 2012a; Nakamura et al., 2011; Polo et al., 2010; Smeenk et al., 2010; Smeenk et al., 2013). Thus, there is significant crosstalk between different histone marks and distinct chromatin remodeling enzymes in coordinating signaling and repair activities within damaged chromatin compartments.

Interestingly, while CHD4 is unique to the NuRD chromatin remodeling complex, SMARCA5 resides in a variety of different complexes, including ACF (consisting of SMARCA5 and ACF1), CHRAC (SMARCA5, ACF1, CHRAC15, and CHRAC17), and RSF (SMARCA5 and RSF1) (Wang et al., 2007). The catalytic subunit SMARCA5 (Lan et al., 2010; Nakamura et al., 2011; Sanchez-Molina et al., 2011; Smeenk et al., 2013), as well as the non-catalytic accessory proteins ACF1, CHRAC15, and CHRAC17 have been implicated in DSB repair (Lan et al., 2010; Sanchez-Molina et al., 2011). Remarkably, the role of the accessory factor RSF1 in the DSB response has not been investigated, although tumors harboring RSF1 amplification display chromosomal instability likely through an altered DDR (Sheu et al., 2010).

Here we uncover RSF1 as a novel factor that is recruited to sites of DSBs and protects human cells against the toxic consequences of IR-induced DSBs. While RSF1 is dispensable for RNF8/

RNF168-dependent ubiquitin signaling of DSBs, it promotes the repair of DSBs by NHEJ and HR. Mechanistically, we show that RSF1 promotes the deposition of the centromere proteins CENP-S and CENP-X at DSBs, which, in turn, promote the assembly of the NHEJ protein XRCC4. Thus, RSF1 is a novel chromatin accessory factor that regulates DSB repair independently of the SMARCA5 ATPase to prevent chromosome aberrations and maintain genome stability.

RESULTS

RSF1 protects cells against DNA damage

The ATPase SMARCA5 forms distinct chromatin remodeling complexes with the chromatin assembly factor ACF1, the histone-fold proteins CHRAC15/CHRCA17 and the remodeling and spacing factor RSF1 (Wang et al., 2007). We and others have recently implicated SMARCA5 in the signaling and repair of DSBs (Lan et al., 2010; Nakamura et al., 2011; Smeenk et al., 2013). However, while the available data suggest that ACF1 and CHRAC15/CHARCA17 assist in modulating SMARCA5 activity, the role of RSF1 in the DNA damage response (DDR) remains unclear. Here we set out to study the role of this protein in the DDR by first addressing whether RSF1 protects human cells against the toxic consequences of ionizing radiation (IR)-induced DSBs. To this end, we transfected human VH10-SV40 cells with siRNAs against either RSF1, the repair factor XRCC4 (positive control), or luciferase (negative control). Cells were subsequently exposed to different doses of IR after which we determined their clonogenic survival capacity. Strikingly, cells depleted for RSF1 were more sensitive to IR than control cells and were nearly as sensitive as XRCC4-depleted cells (Fig. 1A and B), suggesting that RSF1 protects cells against the DSB-inducing effects of ionizing radiation.

RSF1 is recruited to DNA double-strand breaks

Based on this result we reasoned that RSF1 like SMARCA5 and ACF1 may act directly in the DSB response by operating at sites of DNA damage (Lan et al., 2010; Nakamura et al., 2011; Smeenk et al., 2013). To test this we used laser micro-irradiation to examine whether RSF1 directly assembles at sites of DNA damage. DNA damage was induced in a sub-nuclear volume in U2OS cells by multi-photon laser irradiation followed by immunostaining for RSF1 and the DDR factor MDC1, which binds to the DNA damage marker γH2AX. We found that endogenous RSF1 accumulates at sites of laser-induced DNA damage that are marked by MDC1 (Fig. 1C). In addition, we also observed recruitment of GFP-RSF1 to γH2AX-decorated sites following multiphoton-induced laser irradiation in cells stably expressing GFP-RSF1 at near physiological levels (Fig. 1D and E). However, while these results suggest that RSF1 accumulates at DNA lesions we cannot exclude that RSF1 accumulates at lesions other than DSBs given that laser-based approaches have been shown to induce DSBs as well as a variety of other lesions such as single-strand breaks and base damages (Dinant et al., 2007). In order to examine whether RSF1 localizes to bona fide DSBs, we co-expressed GFP-RSF1 and the Fok1 nuclease domain fused to the E. coli lactose repressor (LacR) and the red fluorescent mCherry protein (Fok1-mCherry-LacR) in U2OS cells containing an array of lactose operator (LacO) repeats (Shanbhag et al., 2010). Targeting of Fok1-Cherry-LacR, but not Fok1-Cherry-LacRD450A encoding a nuclease-dead isoform of Fok1, led to DSB induction at the array as visualized by the appearance of γH2AX (Fig. 1F). Importantly, GFP-RSF1 localized to the

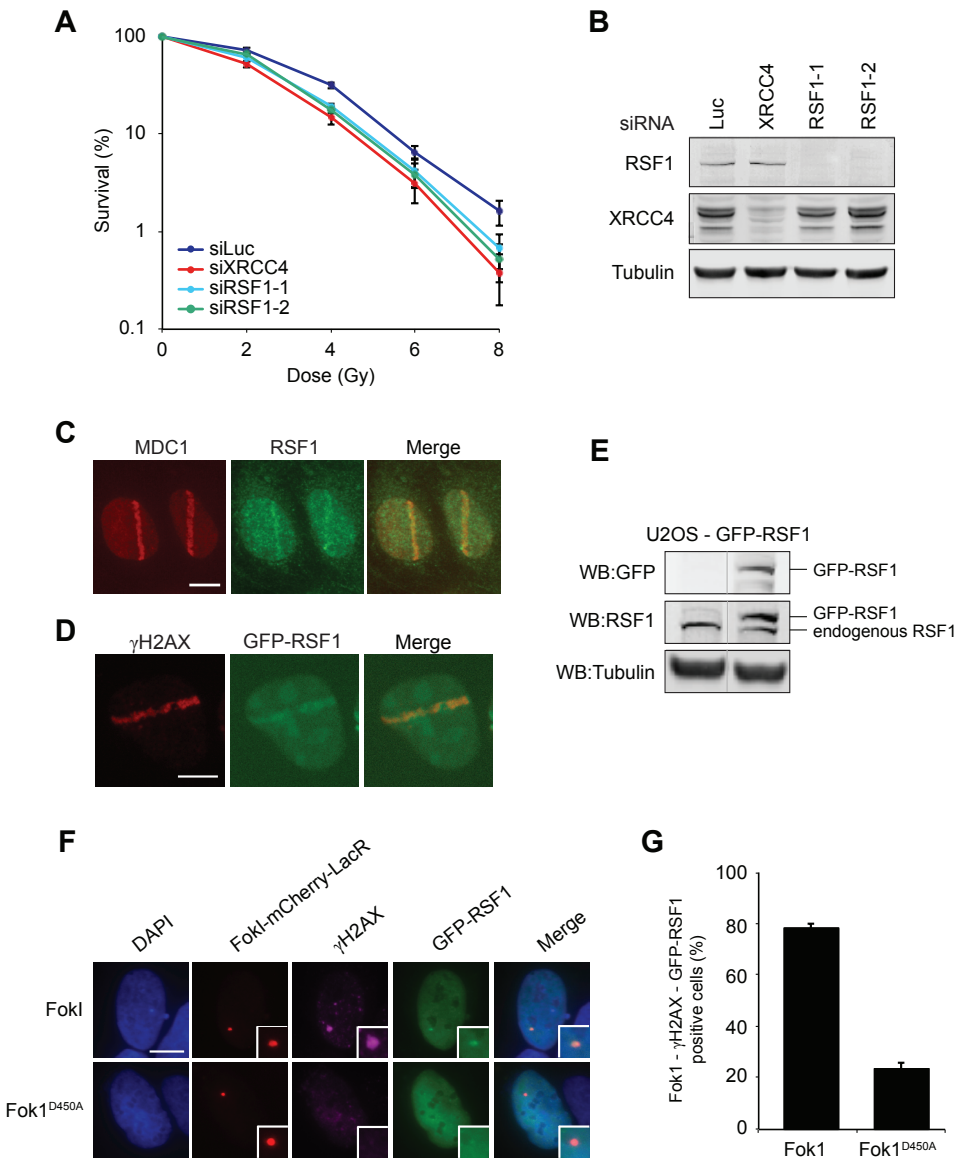

Figure 1. RSF1 protects cells against IR and is recruited to DNA double-strand breaks. (A) VH10-SV40 cells were transfected with the indicated siRNAs, exposed to IR and scored for clonogenic survival. Graphs represent the mean +/- s.e.m. of 3 independent experiments. (B) RSF1 and XRCC4 levels were monitored by western blot analysis using whole cell extracts (WCE) of cells in A. Tubulin is a loading control. (C) U2OS cells were subjected to multiphoton laser irradiation. After 10 min cells were immunostained for endogenous RSF1 and MDC1. Scale bar, 10 µm. (D) As in (C), except that cells stably expressing GFP-RSF1 were used and stained for γH2AX. (E) RSF1 and GFP-RSF1 levels were monitored by western blot analysis using whole cell extracts (WCE) of cells in (D). Tubulin is a loading control. (F) Immunofluorescence staining of γH2AX and visualization of GFP-RSF1 at DSBs induced by Fok1-mCherry–LacR at a tandemly integrated 256× Lac operator genomic array in U2OS cells. Nuclease-deficient FokID450A-mCherry–LacR was used as a control. (G) Quantification of co-localization of γH2AX and GFP-RSF1 at FokI-induced DSBs in cells from (F). Graphs represent the mean +/- s.e.m. of 2 independent experiments. At least 100 individual cells were analyzed. Scale bar, 10 µm.

array upon targeting Fok1, but not upon targeting nuclease dead-Fok1, suggesting that it assembles at Fok1-induced DSBs (Fig. 1F and G). Together, our results show that RSF1 is a novel DDR factor that assembles at DSBs in human cells.

SMARCA5, but not RSF1, regulates the ubiquitin-dependent accumulation of BRCA1 at DSBs

Next, we sought to unravel how RSF1 regulates the DSB response. We recently reported that SMARCA5 regulates the ubiquitin-dependent accumulation of BRCA1 at DSBs (Smeenk et al., 2013). This process is triggered by the MDC1-depedendent recruitment of the RNF8 and RNF168 E3 ubiquitin ligases to DSBs, followed by the ubiquitylation of DSB-flanking chromatin and the subsequent recruitment of the RAP80-BRCA1 complex (Doil et al., 2009; Huen et al., 2007; Mailand et al., 2007; Stewart et al., 2009; Wang and Elledge, 2007). We

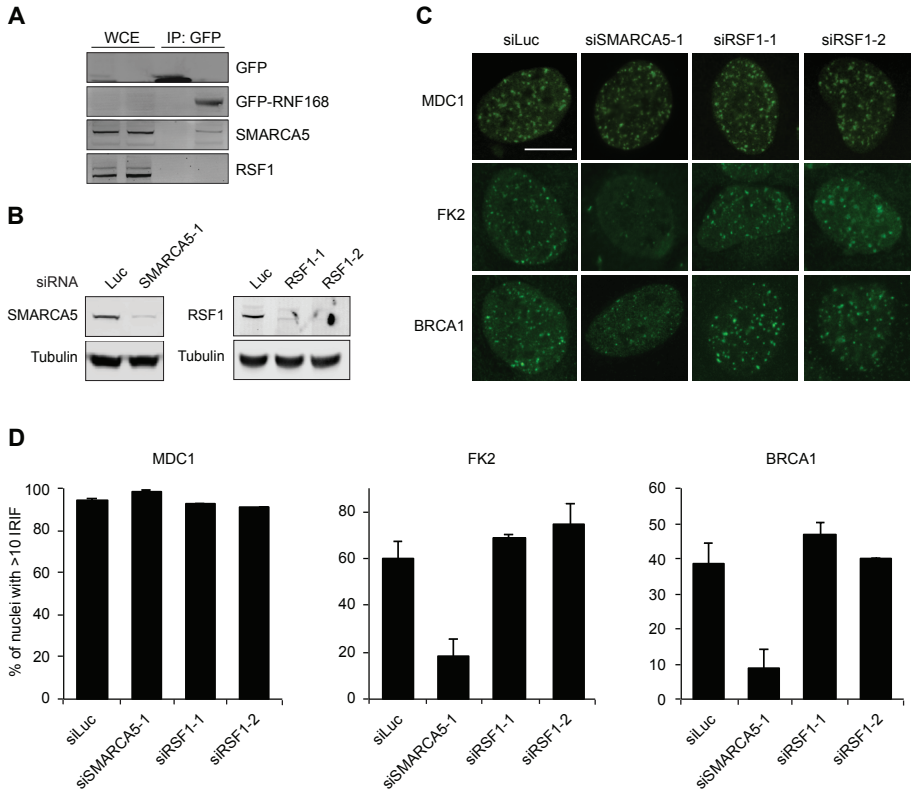

Figure 2. SMARCA5, but not RSF1, associates with RNF168 to regulate the ubiquitin-dependent accumulation of BRCA1 at DSBs. (A) Whole cell extracts (WCE) of U2OS cells expressing either GFP (lane 1 and 3) or GFP-RNF168 (lane 2 and 4) were subjected to GFP immunoprecipitation (IP) followed by western blot analysis of the indicated proteins. GFP-RNF168 expression was too low to be detectable in WCE. (B) U2OS cells were transfected with the indicated siRNAs and subjected to western blot analysis to monitor the efficiency of SMARCA5 and RSF1 knockdown. Tubulin is a loading control. (C) Cells from (B) were exposed to 2 Gy IR or left untreated, and 1 h later immunostained for MDC1, conjugated ubiquitin (FK2) or BRCA1 to visualize ionizing radiation-induced foci (IRIF). Images of untreated cells are presented in Fig. S1A. Scale bar, 10 µm. (D) Quantitative representation of IRIF formation in C. The average percentage of cells with more than 10 IRIF +/- s.e.m. is presented. More than 120 nuclei were scored per sample in 2–3 independent experiments. Quantification of foci in untreated cells is presented in Fig. S1B.

found that SMARCA5 physically associates with RNF168 and affects the BRCA1 response by promoting RNF168-dependent chromatin ubiquitylation (Smeenk et al., 2013). Since RSF1 interacts with SMARCA5 (Perpelescu et al., 2009), we reasoned that it may be part of the RNF168-SMARCA5 complex and as such contribute to this response at the level of RNF168. To test this, we examined whether RSF1, like SMARCA5, associates with the RNF168 E3 ligase. However, although immunoprecipitation of GFP-tagged RNF168 from U2OS cells followed by western blot analysis revealed an interaction with SMARCA5, which is in agreement with our previous observations (Smeenk et al., 2013), we noticed that RNF168 did not interact with RSF1 (Fig. 2A). This suggests that RSF1 is not a constituent of the RNF168-SMARCA5 complex. Supporting the physiological relevance of the observed interactions, we found that depletion of SMARCA5, but not of RSF1, impaired the accumulation of conjugated ubiquitin and BRCA1 into IR-induced foci, whereas MDC1 IRIF formation remained unaffected by the loss of SMARCA5 or RSF1 (Fig. 2B–D; Fig. S1). These results, together with our previous work (Smeenk et al., 2013), suggest that RSF1, in contrast to SMARCA5, does not interact with RNF168 and is dispensable for the ubiquitin-dependent accumulation of BRCA1 at DSBs.

RSF1 regulates DSB repair by homologous recombination and non-homologous end-joining

Given that RSF1 does not affect the RNF168-dependent signaling of DSBs we reasoned that it could be involved in the repair of DSBs. We used two established reporter assays to monitor the role of RSF1 in HR and NHEJ, which are the two major pathways that have evolved to repair DSBs. The DR-GFP reporter for HR is composed of two differentially mutated GFP genes oriented as direct repeats. While the upstream repeat carries a recognition site for the rare-cutting I-SceI endonuclease, the downstream repeat consists of a 5' and 3' truncated GFP gene. Transient expression of I-SceI leads to the induction of a DSB in the upstream GFP gene, which can be repaired by HR using the downstream GFP fragment as a homologous template. Repair by HR following I-SceI cleavage thus results in the restoration of a functional GFP gene and subsequent GFP expression, which can be quantified by flow cytometry (Fig. 3A and C; compare siLuc −/+ I-SceI samples in C) (Weinstock et al., 2006). On the other hand, the EJ5-GFP reporter for NHEJ consists of a GFP gene that is separated from its promoter by the insertion of a Puromycine gene that is flanked by I-SceI recognition sites. Transient expression of I-SceI leads to the induction of DSBs and excision of the Puromycine gene. NHEJ-mediated repair of the broken ends fuses the promoter to the GFP gene, rendering the cells positive for GFP (Fig. 3B) (Bennardo et al., 2008). As expected, depletion of BRCA2, a key factor involved in HR, dramatically reduced the fraction of GFP-positive DR-GFP cells, but not EJ5-GFP cells, whereas depletion of the NHEJ factor XRCC4 reduced the fraction of GFP-positive EJ5-GFP cells (Fig. 3C and D). Importantly, when we depleted RSF1 we observed a significant reduction in the fraction of both GFP-positive DR-GFP and EJ5-GFP cells (Fig. (Fig. 3C–E). As cell cycle profiles remained unchanged after knockdown of RSF1, we can rule out that cell cycle changes affected the HR and NHEJ efficiencies (Fig. S3). Therefore, our results demonstrate that RSF1 promotes efficient DSB repair by both HR and NHEJ.

RSF1 promotes the assembly of CENP-X and CENP-S at damaged chromatin

The RSF complex is required for the incorporation of centromere protein A (CENP-A), a histone H3 variant, into centromeric chromatin (Perpelescu et al., 2009). Interestingly, Zeitlin and colleagues showed that CENP-A accumulates at laser- and nuclease-induced DSBs and proposed a role for CENP-A in DSB repair (Zeitlin et al., 2009). These observations prompted

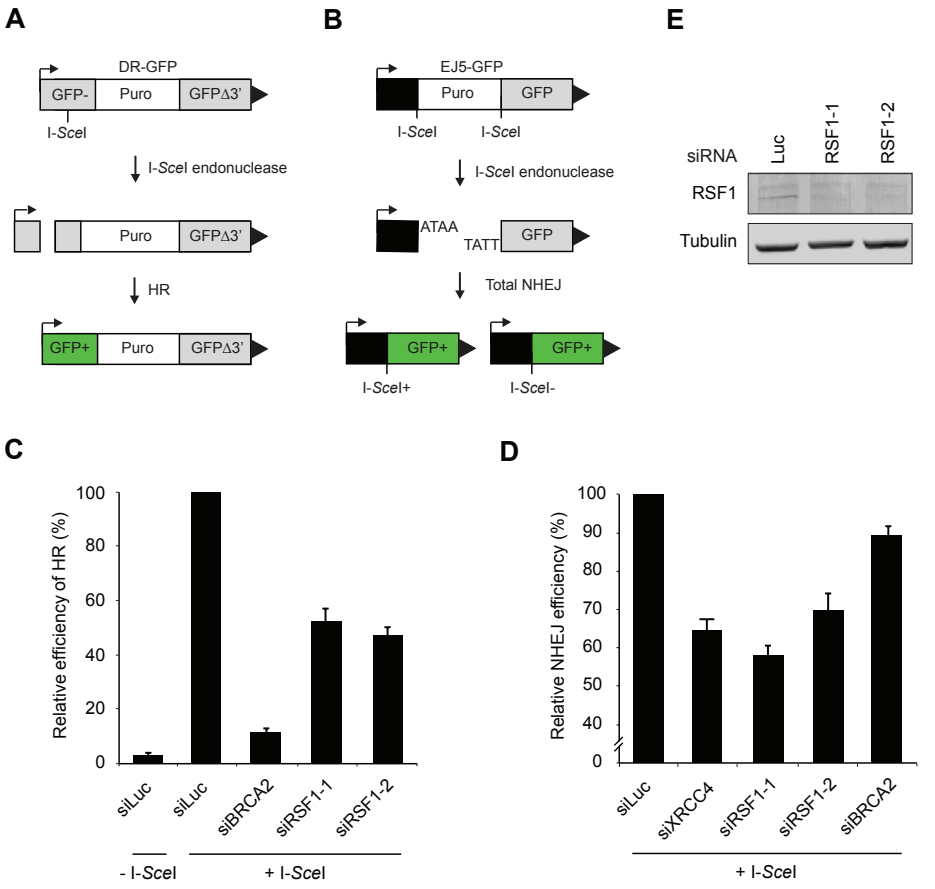

Figure 3. RSF1 regulates DSB repair by homologous recombination and non-homologous end-joining. (A) Schematic of the DR-GFP reporter used to monitor HR in HEK293T cells (see text for details). (B) Schematic of the EJ5-GFP reporter used to monitor NHEJ in HEK293T cells (see text for details). (C) DR-GFP reporter cells were transfected with the indicated siRNAs and 48 h later transfected with an I-SceI expression vector (pCBASce). 48 h later cells were analyzed for GFP expression by flow cytometry. The mean +/- s.e.m. of 4 experiments is shown. (D) As in (C), except that cells containing the NHEJ reporter EJ5-GFP were used. The mean +/- s.e.m. of 3 experiments is shown. (E) Western blot analysis showing the knockdown efficiency for the indicated siRNAs in HEK293T cells used in (C) and (D).

us to investigate whether RSF1, by targeting CENP-A to DNA breaks, could affect DSB repair. However, we failed to detect the accumulation of endogenous CENP-A at sites of DNA damage induced by our multiphoton laser when using irradiation conditions similar to those used to detect RSF1 assembly (Fig. S4A). When using U2OS cells stably expressing GFP-CENP-A, we observed weak GFP-CENP-A accumulation in laser tracks, but only in a very limited number of cells when high laser power was applied (Fig. S4B). In addition, we also found laser tracks in which GFP-CENP-A was excluded (Fig. S4B). Due to the difficulties to detect CENP-A recruitment to DSBs using our multiphoton laser set-up, we concluded that it would be very difficult to experimentally link RSF1 to the targeting of CENP-A to DSBs. Instead, we focused on the possibility that RSF1 may load other centromere proteins onto damaged chromatin. Recently, the centromere proteins CENP-S and CENP-X (also called MHF1 and MHF2) were isolated in a complex with the Fanconi anemia (FA) protein M (FANCM) (Singh et al., 2010;

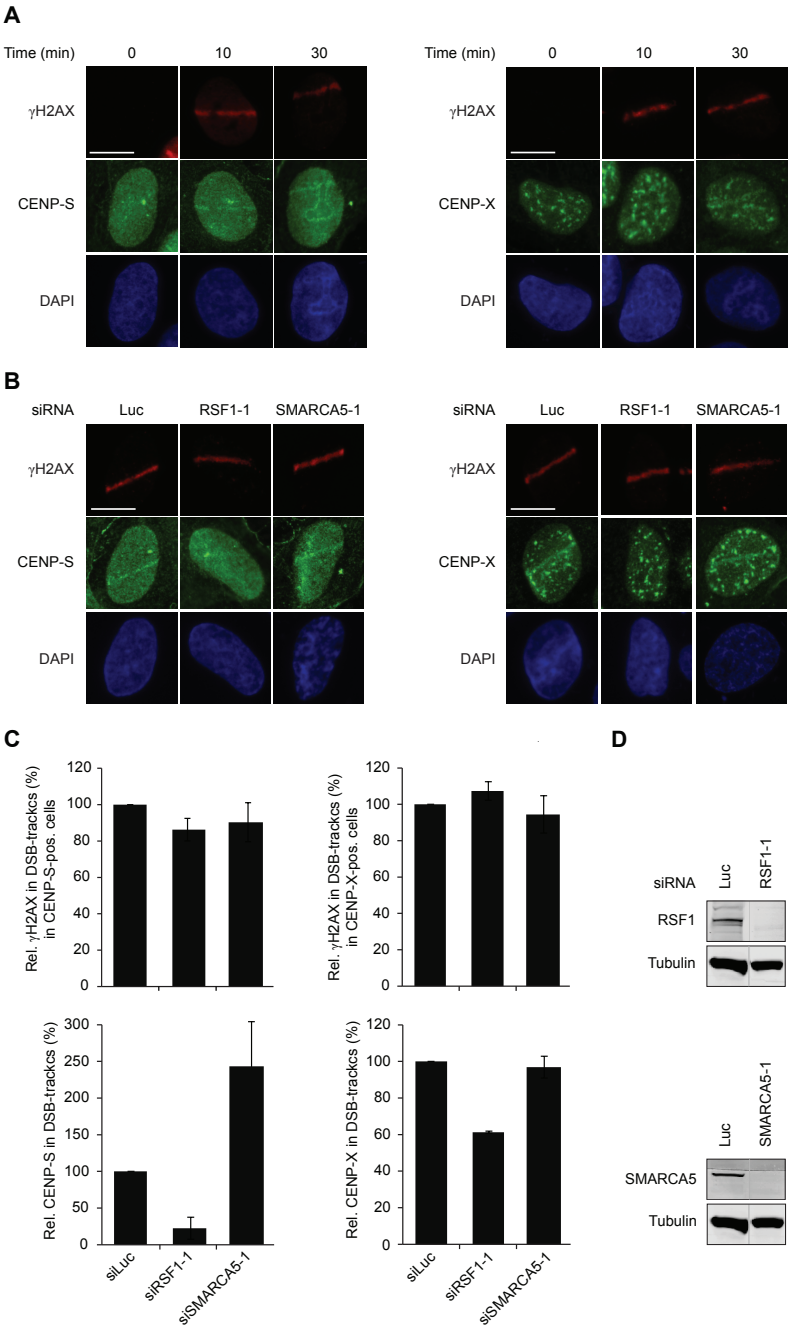

Figure 4. RSF1 promotes the assembly of CENP-S and CENP-X at damaged chromatin. (A) U2OS cells were subjected to multiphoton laser irradiation and immunostained for γH2AX and endogenous CENP-S (left panel) or CENP-X (right panel) at the indicated time-points. Scale bar, 10 µm. (B) As in (A), except that cells were treated with the indicated siRNAs and immunostained at 30 min after laser irradiation. (C) Quantification of the relative levels of γH2AX and CENP-S or CENP-X in laser tracks after transfection with the indicated siRNAs. The levels in siLuc-treated cells (control) were set to 100%. Graphs represent the mean +/- s.e.m. of 40–130 individual cells from 2 independent experiments. (D) Western blot analysis showing the knockdown efficiency for the indicated siRNAs.

Yan et al., 2010). FANCM is a member of the Fanconi core complex that consists of at least seven other components and is required to protect cells against the cytotoxic effects of agents that induce DNA inter-strand crosslinks (ICLs) (Kottemann and Smogorzewska, 2013). Interestingly, CENP-S and CENP-X are required for the loading of FANCM at ICLs, suggesting that these factors play a role in ICL repair (Singh et al., 2010; Yan et al., 2010). However, whether these centromere proteins act in other DNA repair pathways remains unclear. Therefore, we first addressed whether these CENP proteins are recruited to laser-induced DNA damage. Strikingly, we found that following multiphoton laser micro-irradiation both endogenous CENP-S and CENP-X assembled at DSB-containing laser tracks that were marked by γH2AX (Fig. 4A). To verify these results we generated GFP-tagged fusions of both CENP proteins and observed recruitment of GFP-tagged CENP-S and CENP-X to such damaged areas (Fig. S5). Having established that CENP-S and CENP-X accumulate at sites of DNA damage we then asked whether this event requires RSF1. Indeed, we found that RSF1 depletion by two independent siRNAs reduced the accumulation of endogenous CENP-S and CENP-X (Fig. 4B–D). Notably, the stronger centromeric localization of CENP-X compared with CENP-S detected by our antibodies may have obscured its accumulation in laser tracks and therefore complicated quantification. This is likely why the impact of RSF1 depletion on CENP-X appears milder in comparison to the striking reduction of CENP-S accumulation (Fig. 4B–D). Remarkably, however, knockdown of SMARCA5 did not impair the assembly of these centromere proteins at sites of DNA damage, suggesting that RSF1 can act independently of SMARCA5 during the DSB response (Fig. 4B–D). In support of such a scenario, we found that RSF1 and SMARCA5, although recruited to sites of DNA damage with similar kinetics (Fig. S6A and B), assembled independently from each other at DSBs (Fig. S6C–G). Finally, the effect of RSF1 on CENP-S and CENP-X loading was not indirect through transcriptional regulation, as the expression levels of both CENP proteins remained unchanged after RSF1 or SMARCA5 knockdown (Fig. S7A). Together, these results suggest that CENP-S and CENP-X assemble at damaged chromatin in an RSF1-dependent manner, while SMARCA5 is not involved in the loading of these proteins. We infer that CENP-S and CENP-X may be involved in regulating RSF1-dependent DSB repair events.

CENP-S and CENP-X promote NHEJ, but not HR

We next addressed whether we could functionally link the role of RSF1 in promoting DSB repair to its effect on CENP-S and CENP-X loading at DNA lesions. To deplete cells of the centromere proteins CENP-S and CENP-X we used either a single siRNA or a smartpool of siRNAs in the DR-GFP and EJ5-GFP reporter cells. As we could not detect CENP-S and CENP-X on western blots using any of the available antibodies, we established that the siRNAs not only dramatically reduced CENP-S and CENP-X mRNA levels, but also severely reduced the expression of exogenously expressed GFP-tagged CENP-S and CENP-X, demonstrating the functionality and specificity of our siRNAs (Fig. 5A; Fig. S2B). Surprisingly, while we found that depletion of RSF1, similar to that of BRCA2, significantly reduced the levels of GFP-positive DR-GFP cells (Figs. 3C and 5B), we did not observe this phenotype after CENP-S or CENP-X depletion (Fig. 5B). This suggests that RSF1 does not drive DSB repair by HR through loading of CENP-S or CENP-X at DSBs. In contrast, knockdown of CENP-S or CENP-X, similar to that of RSF1 or XRCC4 (Figs. 3D and 5C), significantly reduced the levels of GFP-positive EJ5-GFP cells (Fig. 5C), which suggests that RSF1 may promote DSB repair by NHEJ through regulating the assembly of CENP-S and CENP-X at DSBs.

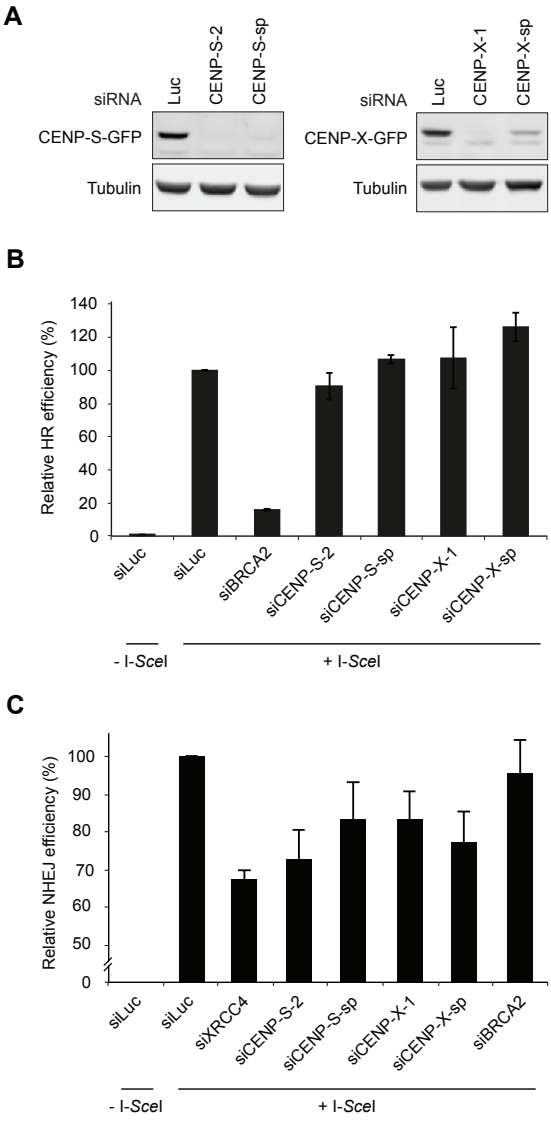

Figure 5. CENP-S and CENP-X promote NHEJ, but not HR. (A) HEK293T cells were treated with the indicated siRNAs and 48 h later transfected with either a GFP-CENP-S or GFP-CENP-X expression vector. Twenty-four h later cells were subjected to western blot analysis to show the knockdown efficiency for the indicated siRNAs. (B) HEK293T cells containing the HR reporter DR-GFP were transfected with the indicated siRNAs and 48 h later transfected with an I-SceI expression vector (pCBASce). Forty-eight h later cells were analyzed for GFP expression by flow cytometry. The mean +/- s.e.m. of 3 experiments is shown. (C) As in (B), except that cells containing the NHEJ reporter EJ5-GFP were used.

RSF1, CENP-S and CENP-X promote the assembly of the NHEJ factor XRCC4

One of the key factors involved in NHEJ is the XRCC4 protein, which forms a stable heterodimer with DNA ligase IV, a protein required for rejoining the broken ends during NHEJ.3 Indeed, we found that endogenous XRCC4 accumulates in DSB-containing laser tracks following UV-A laser micro-irradiation (Fig. 6A; see siLuc control samples). We then asked whether RSF1 and CENP-S and CENP-X would function together to recruit XRCC4 to damaged chromatin. Indeed, we found that depletion of either RSF1, CENP-S, or CENP-X resulted in a significant reduction in DSB-associated XRCC4, while the level of DNA damage induction as monitored by γH2AX formation was comparable in the different knockdown cells (Fig. 6). The effect of RSF1 and the CENP proteins on XRCC4 loading was not indirect through transcriptional regulation as the XRCC4 expression levels remained unchanged in the knockdown cell lines

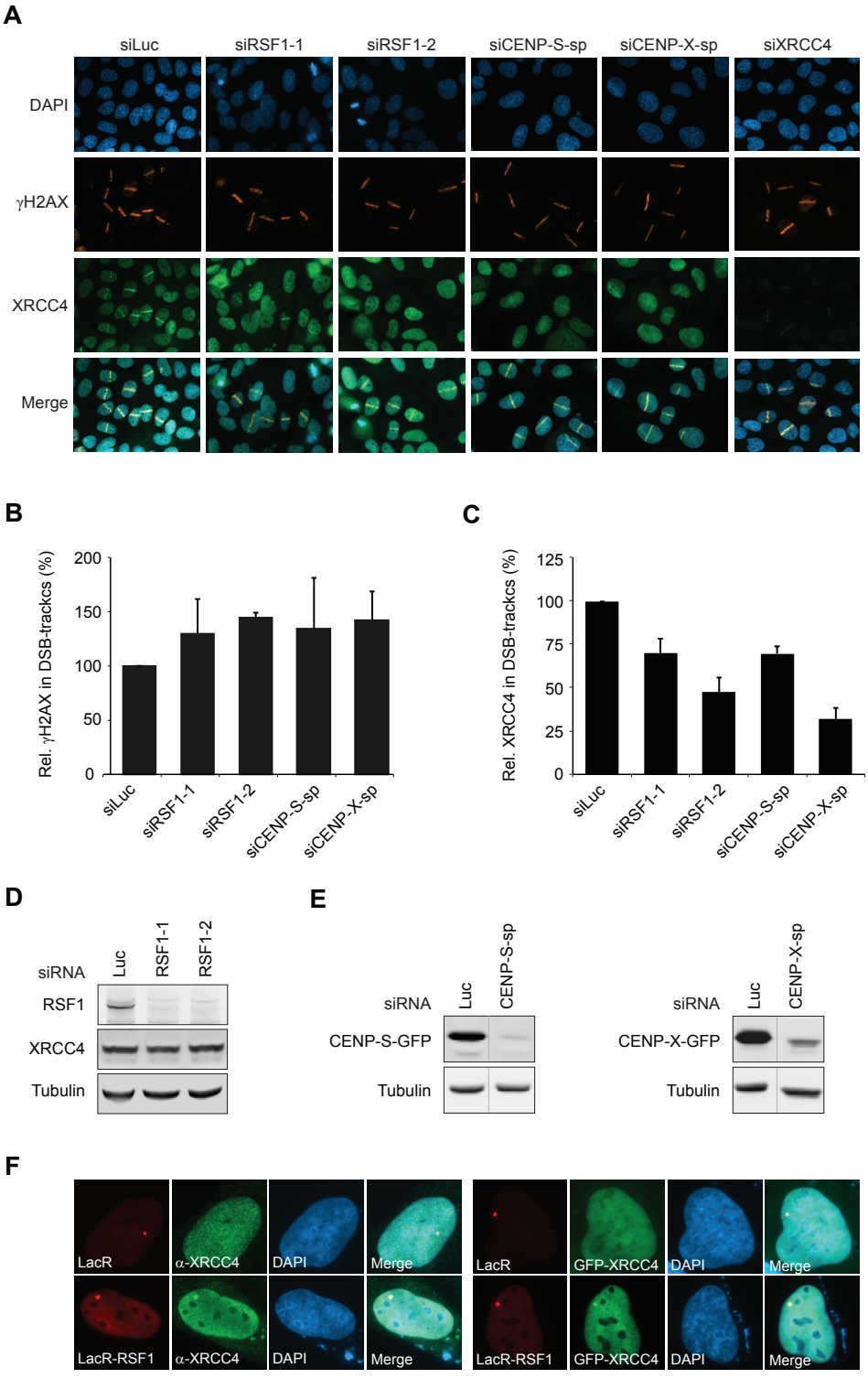
A
siLuc
siRSF1-1
siRSF1-2
siCENP-S-sp
siCENP-X-sp
siXRCC4
DAPI
γH2AX
XRCC4
Merge
B
Rel. γH2AX in DSB-trackcs (%)
200
150
100
50
0
siLuc
siRSF1-1
siRSF1-2
siCENP-S-sp
siCENP-X-sp
C
Rel. XRCC4 in DSB-trackcs (%)
125
100
75
50
25
0
siLuc
siRSF1-1
siRSF1-2
siCENP-S-sp
siCENP-X-sp
D
siRNA
Luc
RSF1-1
RSF1-2
RSF1
XRCC4
Tubulin
E
siRNA
Luc
CENP-S-sp
CENP-S-GFP
Tubulin
siRNA
Luc
CENP-X-sp
CENP-X-GFP
Tubulin
F
LacR
α-XRCC4
DAPI
Merge
LacR
GFP-XRCC4
DAPI
Merge
LacR-RSF1
α-XRCC4
DAPI
Merge
LacR-RSF1
GFP-XRCC4
DAPI
Merge

<
F**igure 6. RSF1, CENP-S and CENP-X load XRCC4 onto damaged chromatin.** (A) U2OS cells were treated with the indicated siRNAs, then subjected to UV-A laser irradiation and 30 min later immunostained for γH2AX and endogenous XRCC4. Scale bar, 10 µm. (B) Quantitative representation of results in (A). The relative levels of γH2AX in laser tracks were plotted. The level of γH2AX in siLuc-treated cells (control) was set to 100%. Graphs represent the mean +/- s.e.m. of at least 60 individual cells from 2 independent experiments. (C) As in (B), except for XRCC4. (D) Western blot analysis showing the knockdown efficiency for the indicated siRNAs in cells from (B) and (C). (E) U2OS cells were treated with the indicated siRNAs and 48 h later transfected with either a CENP-S-GFP or CENP-X-GFP expression vector. Twenty-four h later cells were subjected to western blot analysis to show the knockdown efficiency for the indicated siRNAs in (B and C). (F) U2OS 2–6-3 cells harboring a LacO array were transfected with mCherry-LacR or mCherry-LacR-RSF1 and (left panel) immunostained for endogenous XRCC4 or (right panel) co-transfected with GFP-XRCC4.

(Fig. S7B). Given that RSF1 is required for CENP-S and CENP-X assembly onto damaged chromatin, this suggests that the RSF1, CENP-S and CENP-X proteins collaborate to promote NHEJ by regulating chromatin-bound XRCC4 levels at DSB sites. To provide further evidence for the RSF1-mediated loading of XRCC4, we generated a mCherry-LacR-tagged version of RSF1, which was targeted to a LacO-containing genomic locus in U2OS cells (Luijsterburg et al., 2012a; Luijsterburg et al., 2012b; Soutoglou and Misteli, 2008). Strikingly, endogenous as well as GFP-tagged XRCC4 clearly accumulated at the LacO array upon targeting of LacR-RSF1 to chromatin in virtually all cells examined, while targeting of LacR alone failed to recruit XRCC4 (Fig. 6F). These findings show that prolonged binding of RSF1 to chromatin triggers the recruitment of XRCC4 even in the absence of DSBs. Together, these results suggests that the RSF1-dependent loading of CENP-S and CENP-X at DSB sites promotes the assembly of the XRCC4-DNA ligase IV complex, thereby promoting efficient NHEJ.

DISCUSSION

Here we uncover novel functions for the spacing and remodeling factor 1 (RSF1) protein in the repair of DSBs. RSF1 regulates the two major DSB repair pathways, NHEJ and HR, through distinct mechanisms. At centromeres, RSF1 was shown to deposit the centromere protein CENP-A (Perpelescu et al., 2009). Reminiscent of such a mechanism, we uncovered that in response to genomic insult RSF1 loads the centromere proteins CENP-S and CENP-X onto damaged chromatin. These two factors, in turn, facilitate the efficient assembly of the NHEJ factor XRCC4 to promote repair through NHEJ. Remarkably, CENP-S and CENP-X were dispensable for the function of RSF1 in HR, suggesting an alternative pathway for RSF1-dependent regulation of HR, which remains to be elucidated but may involve the reported functional interaction between RSF1 and cyclin proteins involved in DSB repair (Jirawatnotai et al., 2011). Thus, RSF1 is a critical factor involved in the efficient execution of the two major pathways of DSB repair.

SMARCA5, but not RSF1 is linked to RNF168-dependent signaling of DSBs

While it is evident from our studies that RSF1 regulates DSB repair, we did not uncover a role for this protein in the ubiquitin-dependent BRCA1 response pathway. This result is surprising given that we have previously shown that the RSF1-associated ATPase SMARCA5 directly interacts with ubiquitin ligase RNF168 and is essential for the DNA damage-induced conjugation of ubiquitin and subsequent BRCA1 accumulation at DSBs (Smeenk et al., 2013). However, SMARCA5 resides in different multi-protein complexes and it may be that complexes other than the RSF complex (e.g., ACF or CHRAC) regulate the RNF168-

driven response at DSBs. On the other hand, it is interesting to note that several SMARCA5-associated non-canonical subunits appear to have distinct SMARCA5-independent functions in the DDR. For instance, ACF1 was previously shown to regulate the recruitment of the NHEJ factors KU70/80 to DSBs, while this event did not require SMARCA5 (Lan et al., 2010). In this study, we report that RSF1 is recruited independently from SMARCA5 to DSBs and regulates the assembly of centromere proteins CENP-S and CENP-X in a manner that did not require SMARCA5.

CENP-S and CENP-X: Novel factors involved in DSB repair

We found that RSF1 promotes DSB repair by both NHEJ and HR. Our data suggest that RSF1 regulates NHEJ by recruiting CENP-S and CENP-X to DSB-associated chromatin, which in turn promotes assembly of the XRCC4-LigIV complex. It is currently not clear whether RSF1 promotes CENP-S/CENP-X assembly through recruiting CENP-A, or whether RSF1 directly loads CENP-S/CENP-X onto damaged chromatin. In addition, how CENP-S and CENP-X assembly contributes to XRCC4 binding at DSB sites remains to be elucidated. Previous studies demonstrated that CENP-S and CENP-X form a compact tetramer that can bind DNA and resembles H3-H4 tetramers found in histone octamers (Nishino et al., 2012; Tao et al., 2012). CENP-S and CENP-X localize to centromeres where they promote the assembly of kinetochore proteins (Amano et al., 2009; Foltz et al., 2006). Consequently, loss of either CENP-S or CENP-X leads to mitotic abnormalities and genome instability (Amano et al., 2009). However, CENP-S and CENP-X function does not seem to be restricted to centromeres. Recently, the FANCM protein was found to associate with the CENP-S – CENP-X tetramer. Moreover, CENP-S and CENP-X appeared to be important for the accumulation of FANCM at psoralen-induced ICL, indicating that CENP-S and CENP-X may function at genomic sites other than centromeres (Singh et al., 2010; Yan et al., 2010). Here we extend the repertoire of genomic locations at which CENP-S and CENP-X could execute their function by showing that these factors assemble at DSB-containing laser tracks.

CENP proteins, chromatin structure and DSB repair

Analogous to their function at ICLs, it is possible that these CENP proteins may also target FANCM to DSBs sites, although it is currently unclear whether FANCM is involved in the IR-induced DSB response. On the other hand, our results suggest that the CENP-S/CENP-X complex may functionally interact with factors other than FANCM, such as the NHEJ factor XRCC4. To this end, it would be interesting to investigate whether XRCC4, either directly or indirectly, is able to associate with the CENP-S – CENP-X tetramer and whether this physical connection is important for its relocation to DSB sites. However, we can also not exclude the possibility that CENP-S and CENP-X by modulating chromatin structure affect the retention of XRCC4 at DSB sites. The available data suggest that CENP-S and CENP-X are not incorporated into nucleosomes. Rather, the CENP-S – CENP-X tetramer itself may bind to DNA nucleosome-free regions (Nishino et al., 2012; Tao et al., 2012), including those that are in close proximity to DSBs. The binding of CENP proteins to DNA may enhance the binding of DNA repair factors such as XRCC4, which possess DNA-binding properties, possibly through cooperative interactions on the DNA. Finally, CENP-S and CENP-X also form a stable complex with two other centromere proteins known as CENP-T and CENP-W. The CENP-T-W-X-S complex can bind DNA and form nucleosome-like structures (Nishino et al., 2012). Given that CENP-T, like CENP-S and CENP-X, is recruited to sites of DNA damage (Zeitlin et al., 2009), we cannot rule out the possibility that this complex associates with

damaged chromatin to modulate its structure and facilitates binding of repair factors such as XRCC4. Biochemical studies will be required to further study the importance of the CENP-T-W-X-S complex in modulating chromatin structure at sites of DNA damage.

RSF1, CENP-S and CENP-X in ICL repair and cancer

CENP-S and CENP-X have been suggested to play a role in the FANCM-dependent repair of ICLs by recruiting this FA protein to such lesions. However, how the assembly of CENP-S and CENP-X at ILCs is regulated remains unclear. Here we identify RSF1 as a novel factor that loads CENP-S and CENP-X at sites of DNA damage. Future studies may uncover whether RSF1 is also responsible for CENP-S and CENP-X loading at sites of ICLs and plays a role in the repair of ICLs along with FA proteins such as FANCM. Overexpression of RSF1 is found in many types of cancer and is correlated with poor prognosis (Sheu et al., 2010; Shih et al., 2005). It would be of interest to study if higher levels of RSF1 in such tumors affect the equilibrium between the different SMARCA5 complexes. An increased abundance of SMARCA5-RSF1 complexes at the expense of other SMARCA5-containing complexes (e.g., ACF or CHRAC) may impact DNA damage-induced ubiquitin signaling. Moreover, given that lower levels of RSF1 clearly impact repair through NHEJ and HR, it is feasible that increased RSF1 levels may affect DSB repair pathway choice and even lead to DSB repair defects in tumors overexpressing RSF1. Given the known synthetic lethality between HR defects and chemical inhibitors of poly(ADP-ribose)polymerase (PARP), this could make RSF1 a potential candidate for PARP inhibitor-based cancer treatment (Helleday, 2011). In summary, our results identify RSF1 as a novel factor that regulates DSB repair and outline a molecular mechanism for the RSF1-mediated assembly of centromere proteins at DSBs to promote non-homologous end-joining.

MATERIAL AND METHODS

Cell culture

U2OS, HEK293 and VH10-SV40-immortalized fibroblast cells were grown in DMEM (Gibco) containing 10% FCS (Bodinco BV) unless stated otherwise. U2OS cells stably expressing GFP-RNF168 and U2OS 2–6–3 cells containing 200 copies of a LacO-containing cassette (~4 Mbp) were gifts from Jiri Lukas and Susan Janicki (Doil et al., 2009; Shanbhag et al., 2010). U2OS cells stably expressing GFP-RSF1 were generated by selection on G418 (100 µg/ml).

Plasmids

Fok1-mCherry-LacR, Fok1-mCherry-LacRD450A and GFP-CENP-A expression vectors were obtained from Roger Greenberg and Don Cleveland (Shanbhag et al., 2010; Zeitlin et al., 2009). GFP-XRCC4 was obtained from Penny Jeggo (Girard et al., 2004). The cDNA for human RSF1 (Open Biosystems, pENTR223.1) was cloned into pDEST-EGFP-C1-STOP, a kind gift of Dr Jason Swedlow, using the GATEWAY® system. The cDNA for human RSF1 was also cloned into mCherry-LacR-C1 (Coppotelli et al., 2013). CENP-S and CENP-X cDNAs were amplified from plasmids that were kindly provided by Iain Cheeseman (Amano et al., 2009), and cloned into pEGFP-C1 and pEGFP-N1 (Addgene).

Transfections and RNAi interference

siRNA and plasmid transfections were performed using HiPerfect (Qiagen), Lipofectamine

RNAiMAX (Invitrogen), Lipofectamine 2000 (Invitrogen), and JetPEI (Polyplus Transfection), respectively, according to the manufacturer's instructions. The following siRNA sequences were used:

5'-CGUACGCGGAAUACUUCGA-3' (Luciferase),
5'-GGAAAGACAUCUCUACUAU-3' (RSF1-1, Dharmacon),
5'-UAAAUGAUCUGGACAGUGA-3' (RSF1-2, Dharmacon),
5'-AGACAAAGGAAGAGAGCTA-3' (RSF1-3, Dharmacon),
5'-GGAUUAAACUGGCUCAUUU-3' (SMARCA5-1, Dharmacon),
5'-GAGGAGAUGUAAUACCUUA-3' (SMARCA5-2, Dharmacon),
5'-GGAAUGGUAUACUCGGAUA-3' (SMARCA5-3, Dharmacon),
5'-GGGCAAAUAGAUUCGAGUA-3' (SMARCA5-6, Dharmacon),
5'-AUAUGUUGGUGAACUGAGA-3' (XRCC4, (Sartori et al., 2007)),
5'-GAAGAAUGCAGGUUUAAUA-3' (BRCA2, MWG),
5'-AGAUUAACCUAGAACGAAA-3' (CENP-S-2, Dharmacon),
5'-GGAAGGAGCUGGUGAGCAG-3' (CENP-X-1, Dharmacon).

In addition, SMARTpools of siRNAs against CENP-S or CENP-X were used (Dharmacon). Cells were transfected twice with siRNAs (40 or 80 nM) within 24 h and examined further 48 h after the second transfection unless stated otherwise.

Generation of DSBs
IR was delivered by a YXlon X-ray generator (YXlon International, 200 KV, 4 mA, dose rate 1.1 Gy/min).

Cell survival assay
VH10-SV40 cells were transfected with siRNAs, trypsinized, seeded at low density, and exposed to IR. Seven days later cells were washed with 0.9% NaCl and stained with methylene blue. Colonies of more than 10 cells were scored.

Fok1 assays
RSF1 localization at FokI-induced DSBs was examined essentially as described (Costelloe et al., 2012; Shanbhag et al., 2010). Briefly, U2OS 2-6-3 cells were co-transfected with GFP-RSF1 and either Fok1-mCherry-LacR, or Fok1-mCherry-LacRD450A. Twenty-four hours later cells were fixed, immunostained for γH2AX and examined microscopically for co-localization of γH2AX, GFP-RSF1, and mCherry-LacR fused to either Fok1 or Fok1D450A using Zeiss AxioImager M2 and D2 widefield fluorescence microscopes.

Laser micro-irradiation
Multiphoton laser micro-irradiation was performed on a Leica SP5 confocal microscope equipped with an environmental chamber set to 37 °C and 5% CO2 as described (Smeenk et al., 2010; Smeenk et al., 2013; Vyas et al., 2013). Briefly, U20S cells were grown on MatTek glass bottom dishes. Media was replaced with colorless DMEM supplemented with 10% FCS and penicillin/streptomycin before imaging. DSB-containing tracks (1.5 μm width) were generated with a Mira modelocked Ti:Sapphire laser (λ = 800 nm, pulselength = 200 fs, repetition rate = 76 MHz, output power = 80 mW). Typically, an average of 75 cells was micro-irradiated (1 iteration per pixel) within 10 min using LAS-AF software. For live cell

imaging, confocal images were recorded before and after laser irradiation at different time intervals. For UV-A laser micro-irradiation U2OS cells were grown on 18 mm coverslips and sensitized with 10 μM 5-bromo-2-deoxyuridine (BrdU) for 24 h, as described (Acs et al., 2011; Luijsterburg et al., 2012a). For micro-irradiation, the cells were placed in a Chamlide TC-A live-cell imaging chamber that was mounted on the stage of a Leica DM IRBE widefield microscope stand (Leica) integrated with a pulsed nitrogen laser (Micropoint Ablation Laser System; Photonic Instruments, Inc). The pulsed nitrogen laser (16 Hz, 364 nm) was directly coupled to the epifluorescence path of the microscope and focused through a Leica 40× HCX PLAN APO 1.25–0.75 oil-immersion objective. The growth medium was replaced by CO2-independent Leibovitz L15 medium supplemented with 10% FCS and pen/strep and cells were kept at 37 °C. The laser output power was set to 78 to generate strictly localized sub-nuclear DNA damage. Following micro-irradiation, cells were incubated for the indicated time-points at 37 °C in Leibovitz L15 and subsequently fixed with 4% formaldehyde before immunostaining. Typically, an average of 50 cells was micro-irradiated (2 iterations per pixel) within 10–15 min using Andor IQ software.

Microscopy analysis

Images of fixed samples were acquired on a Zeiss AxioImager M2 or D2 widefield fluorescence microscope equipped with 40×, 63×, and 100× PLAN APO (1.4 NA) oil-immersion objectives (Zeiss) and an HXP 120 metal-halide lamp used for excitation. Fluorescent probes were detected using the following filters: DAPI (excitation filter: 350/50 nm, dichroic mirror: 400 nm, emission filter: 460/50 nm), GFP/Alexa 488 (excitation filter: 470/40 nm, dichroic mirror: 495 nm, emission filter: 525/50 nm), mCherry (excitation filter: 560/40 nm, dichroic mirror: 585 nm, emission filter: 630/75 nm), Alexa 555 (excitation filter: 545/25 nm, dichroic mirror: 565 nm, emission filter: 605/70 nm), Alexa 647 (excitation filter: 640/30 nm, dichroic mirror: 660 nm, emission filter: 690/50 nm). Images were recorded using ZEN 2012 software and IRIF were scored by eye or by using home-made Stacks software as described (Smeenk et al., 2010; Smeenk et al., 2013). Images recorded after multi-photon- and UV-laser micro-irradiation and immunofluorescence stainings were analyzed using ImageJ. The average pixel intensity of laser tracks induced by either the multi-photon- or the UV-A laser system was measured within the locally irradiated area (Idamage), in the nucleoplasm outside the locally irradiated area (Inucleoplasm) and in a region not containing cells in the same field of view (Ibackground) using ImageJ. The relative level of accumulation expressed relative to the protein level in the nucleoplasm was calculated as follows: ((Idamage − Ibackground)/(Inucleoplasm − Ibackground) – 1). The accumulation in the control cells transfected with siLuc within each experiment was normalized to 100%. Images obtained from live cell imaging after multi-photon micro-irradiation were analyzed using LAS-AF software. Fluorescence intensities were subtracted by the pre-bleach values and normalized to the first data point, which was set to 0, to obtain relative fluorescence units (RFU). The average reflects the quantification of between 50–150 cells from 2–3 independent experiments.

Antibodies

Immunofluorescence and western blot analysis were performed using antibodies against γH2AX, α-Tubulin (Sigma), GFP (Roche), ubiquitin (FK2, Enzo Life Sciences), BRCA1 (Calbiochem and Santa Cruz), MDC1 (Abcam), and SMARCA5/SNF2h (Abcam). The antibodies against RSF1 (Perpelescu et al., 2009), CENP-S and CENP-X (Yan et al., 2010), and XRCC4 were gifts from Kinya Joda, Weidong Wang, Roland Kanaar and Mauro Modesti.

Immunofluorescent labeling

Immunofluoresecent labeling of γH2AX, RSF1, MDC1, FK2, BRCA1, CENP-S, CENP-X, and XRCC4 was performed as described previously (Luijsterburg et al., 2012a; Luijsterburg et al., 2012b; Smeenk et al., 2010; Smeenk et al., 2013). Briefly, cells were grown on glass coverslips and treated as indicated in the figure legends. Subsequently, cells were either washed with PBS (for immunostaining of γH2AX, RSF1, MDC1, FK2, BRCA1, XRCC4) or pre-extracted with 0.25% Triton X-100 in cytoskeletal (CSK) buffer (10 mM Hepes-KOH, 300 mM Sucrose, 100 mM NaCl, 3 mM MgCl2, pH 7.4) on ice for 5 min (for immunostaining of CENP-S and -X), fixed with 4% formaldehyde for 10 min and 0.25% Triton X-100 or NP-40 in PBS for 5 min. Cells were rinsed with phosphate-buffered saline (PBS) and equilibrated in WB (PBS containing 5 g BSA/L, 1.5 g glycine/L) prior to immunostaining, except for immunostaining of XRCC4, cells were equilibrated in a different WB (PBS containing 0.5% BSA and 0.05% Tween 20) and then treated with 100 mM glycine in PBS for 10 min to block unreacted aldehyde groups. Detection was done using goat anti-mouse or goat anti-rabbit IgG coupled to Alexa 488, 555 or 647 (Invitrogen Molecular probes). Samples were incubated with 0.1 µg/ml DAPI and mounted in Polymount.

Protein interaction studies

To study RNF168 interactions, cells were lysed in EBC buffer (50 mM Tris, pH 7.5, 150 mM NaCl, 0.5% NP-40, 1 mM EDTA) supplemented with protease and phosphatase inhibitor cocktails. Cleared lysates were subjected to immunoprecipitation with GFP Trap beads (Chromotek) for 1.5 h. Beads were washed 4 times with EBC buffer and boiled in sample buffer. Bound proteins were resolved by SDS-PAGE and processed for immunoblotting.

Homologous recombination and non-homologous end-joining assays

HEK293 cell lines containing either a stably integrated copy of the DR-GFP or EJ5-GFP reporter were used to measure the repair of I-SceI-induced DSBs by HR or NHEJ, respectively (Bennardo et al., 2008; Pierce et al., 1999). Briefly, 48 h after siRNA transfection, cells were transfected with the I-SceI expression vector pCBASce and a RFP expression vector (Pierce et al., 1999). 48 h later the fraction of GFP-positive cells among the RFP-positive cells was determined by FACS on a BD LSRII flow cytometer (BD Bioscience) using FACSDiva software version 5.0.3. Quantifications were performed using WinMDI 2.9 software.

Cell cycle profiling

For cell cycle analysis cells were fixed in 70% ethanol, followed by DNA staining with 50 µg/ml propidium iodide in the presence of RNase A (0.1 mg/ml). Cell sorting was performed on a flow cytometer (LSRII; BD) using FACSDiva software (version 5.0.3; BD). Quantifications were performed using WinMDI software (version 2.9; J. Trotter).

RNA isolation, cDNA synthesis, and quantitative PCR

RNA was isolated using the miRNeasy minikit (Qiagen). cDNA was generated with the RevertAid first strand cDNA synthesis kit (Thermo scientific) using polydT primers and 1 µg of total RNA as input. After cDNA synthesis, all samples were treated with 1 u RNase H (Life Technologies) for 20 min at 37 °C and diluted 1:10 in water. Realtime qPCR was performed in duplicate on the CFX96/384 system using SYBR green mastermix (Bio-Rad). Cycling conditions: initial melting at 95 °C for 3 min, 40 cycles of 95 °C for 10 s, and 60 °C for 30 s, followed by melting curve analysis (65 °C to 95 °C, stepwise increment of 0.5 °C) to control product specificity. Each reaction contained 4 µl of diluted cDNA and 0.75 pM of each primer

in a total volume of 10 µl. All primer pairs were designed using Primer3Plus software (http://primer3plus.com), tested for efficiency and are listed in Table S1. Relative expression levels were obtained with the CFX manager (vs 3.0), correcting for primer efficiencies and using GAPDH and GUSB as reference genes, unless indicated otherwise.

ACKNOWLEDGMENTS

We would like to thank Noel Lowndes for sharing unpublished data and Jiri Lukas, Susan Janicki, Roger Greenberg, Kinya Joda, Weidong Wang, Roland Kanaar, Mauro Modesti, Penny Jeggo, Jason Swedlow, Jeremy Stark, and Maria Jasin for generously providing valuable reagents. We acknowledge Willem Sloos, Annelies van der Laan, and Hans Tanke for assistance with the laser micro-irradiation experiments. This work was funded by an LUMC Epigenetics grant to ACO and HvA, a VIDI grant from the Netherlands Organization for Scientific Research (NWO) and a CDA grant from HFSP to HVA, and a VENI grant from NWO to MSL.

REFERENCES

1. Acs,K., Luijsterburg,M.S., Ackermann,L., Salomons,F.A., Hoppe,T., and Dantuma,N.P. (2011). The AAA-ATPase VCP/p97 promotes 53BP1 recruitment by removing L3MBTL1 from DNA double-strand breaks. Nat. Struct. Mol. Biol. 18, 1345-1350.
2. Amano,M., Suzuki,A., Hori,T., Backer,C., Okawa,K., Cheeseman,I.M., and Fukagawa,T. (2009). The CENP-S complex is essential for the stable assembly of outer kinetochore structure. J. Cell Biol. 186, 173-182.
3. Bennardo,N., Cheng,A., Huang,N., and Stark,J.M. (2008). Alternative-NHEJ is a mechanistically distinct pathway of mammalian chromosome break repair. PLoS. Genet. 4, e1000110.
4. Chapman,J.R., Taylor,M.R., and Boulton,S.J. (2012). Playing the end game: DNA double-strand break repair pathway choice. Mol. Cell 47, 497-510.
5. Ciccia,A. and Elledge,S.J. (2010). The DNA damage response: making it safe to play with knives. Mol. Cell 40, 179-204.
6. Coppotelli,G., Mughal,N., Callegari,S., Sompallae,R., Caja,L., Luijsterburg,M.S., Dantuma,N.P., Moustakas,A., and Masucci,M.G. (2013). The Epstein-Barr virus nuclear antigen-1 reprograms transcription by mimicry of high mobility group A proteins. Nucleic Acids Res. 41, 2950-2962.
7. Costelloe,T., Louge,R., Tomimatsu,N., Mukherjee,B., Martini,E., Khadaroo,B., Dubois,K., Wiegant,W.W., Thierry,A., Burma,S., van,A.H., and Llorente,B. (2012). The yeast Fun30 and human SMARCAD1 chromatin remodellers promote DNA end resection. Nature 489, 581-584.
8. Dinant,C., de,J.M., Essers,J., van Cappellen,W.A., Kanaar,R., Houtsmuller,A.B., and Vermeulen,W. (2007). Activation of multiple DNA repair pathways by sub-nuclear damage induction methods. J. Cell Sci. 120, 2731-2740.
9. Doil,C., Mailand,N., Bekker-Jensen,S., Menard,P., Larsen,D.H., Pepperkok,R., Ellenberg,J., Panier,S., Durocher,D., Bartek,J., Lukas,J., and Lukas,C. (2009). RNF168 binds and amplifies ubiquitin conjugates on damaged chromosomes to allow accumulation of repair proteins. Cell 136, 435-446.
10. Foltz,D.R., Jansen,L.E., Black,B.E., Bailey,A.O., Yates,J.R., III, and Cleveland,D.W. (2006). The human CENP-A centromeric nucleosome-associated complex. Nat. Cell Biol. 8, 458-469.
11. Girard,P.M., Kysela,B., Harer,C.J., Doherty,A.J., and Jeggo,P.A. (2004). Analysis of DNA ligase IV mutations found in LIG4 syndrome patients: the impact of two linked polymorphisms. Hum. Mol. Genet. 13, 2369-2376.
12. Helleday,T. (2011). The underlying mechanism for the PARP and BRCA synthetic lethality: clearing up the misunderstandings. Mol. Oncol. 5, 387-393.
13. Huen,M.S., Grant,R., Manke,I., Minn,K., Yu,X., Yaffe,M.B., and Chen,J. (2007). RNF8 transduces the DNA-damage signal via histone ubiquitylation and checkpoint protein assembly. Cell 131, 901-914.
14. Jackson,S.P. and Bartek,J. (2009). The DNA-damage response in human biology and disease. Nature 461, 1071-1078.
15. Jirawatnotai,S., Hu,Y., Michowski,W., Elias,J.E., Becks,L., Bienvenu,F., Zagozdzon,A., Goswami,T., Wang,Y.E., Clark,A.B., Kunkel,T.A., van,H.T., Xia,B., Correll,M., Quackenbush,J., Livingston,D.M., Gygi,S.P., and Sicinski,P. (2011). A function for cyclin D1 in DNA repair uncovered by protein interactome analyses in human cancers. Nature 474, 230-234.
16. Kottemann,M.C. and Smogorzewska,A. (2013). Fanconi anaemia and the repair of Watson and Crick DNA crosslinks. Nature 493, 356-363.
17. Lan,L., Ui,A., Nakajima,S., Hatakeyama,K., Hoshi,M., Watanabe,R., Janicki,S.M., Ogiwara,H., Kohno,T., Kanno,S., and Yasui,A. (2010). The ACF1 complex is required for DNA double-strand break repair in human cells. Mol. Cell 40, 976-987.
18. Larsen,D.H., Poinsignon,C., Gudjonsson,T., Dinant,C., Payne,M.R., Hari,F.J., Rendtlew Danielsen,J.M., Menard,P., Sand,J.C., Stucki,M., Lukas,C., Bartek,J., Andersen,J.S., and Lukas,J. (2010). The chromatin-remodeling factor CHD4 coordinates signaling and repair after DNA damage. J. Cell Biol. 190, 731-740.
19. Luijsterburg,M.S., Acs,K., Ackermann,L., Wiegant,W.W., Bekker-Jensen,S., Larsen,D.H., Khanna,K.K., van Attikum,H., Mailand,N., and Dantuma,N.P. (2012a). A new non-catalytic role for ubiquitin ligase RNF8 in unfolding higher-order chromatin structure. EMBO J. 31, 2511-2527.
20. Luijsterburg,M.S., Lindh,M., Acs,K., Vrouwe,M.G., Pines,A., van Attikum,H., Mullenders,L.H., and Dantuma,N.P. (2012b). DDB2 promotes chromatin decondensation at UV-induced DNA damage. J. Cell Biol. 197, 267-281.
21. Luijsterburg,M.S. and van Attikum,H. (2011). Chromatin and the DNA damage response: the cancer connection. Mol. Oncol. 5, 349-367.
22. Mailand,N., Bekker-Jensen,S., Faustrup,H., Melander,F., Bartek,J., Lukas,C., and Lukas,J. (2007). RNF8 ubiquitylates histones at DNA double-strand breaks and promotes assembly of repair proteins. Cell 131, 887-900.
23. Nakamura,K., Kato,A., Kobayashi,J., Yanagihara,H., Sakamoto,S., Oliveira,D.V., Shimada,M., Tauchi,H., Suzuki,H., Tashiro,S., Zou,L., and Komatsu,K. (2011). Regulation of homologous recombination by RNF20-dependent H2B ubiquitination. Mol. Cell 41, 515-528.
24. Nishino,T., Takeuchi,K., Gascoigne,K.E., Suzuki,A., Hori,T., Oyama,T., Morikawa,K., Cheeseman,I.M., and Fukagawa,T. (2012). CENP-T-W-S-X forms a unique centromeric chromatin structure with a histone-like fold. Cell 148, 487-501.
25. Perpelescu,M., Nozaki,N., Obuse,C., Yang,H., and Yoda,K. (2009). Active establishment of centromeric CENP-A chromatin by

RSF complex. J. Cell Biol. 185, 397-407.
26. Pierce,A.J., Johnson,R.D., Thompson,L.H., and Jasin,M. (1999). XRCC3 promotes homology-directed repair of DNA damage in mammalian cells. Genes Dev. 13, 2633-2638.
27. Polo,S.E., Kaidi,A., Baskcomb,L., Galanty,Y., and Jackson,S.P. (2010). Regulation of DNA-damage responses and cell-cycle progression by the chromatin remodelling factor CHD4. EMBO J. 29, 3130-3139.
28. Sanchez-Molina,S., Mortusewicz,O., Bieber,B., Auer,S., Eckey,M., Leonhardt,H., Friedl,A.A., and Becker,P.B. (2011). Role for hACF1 in the G2/M damage checkpoint. Nucleic Acids Res. 39, 8445-8456.
29. Sartori,A.A., Lukas,C., Coates,J., Mistrik,M., Fu,S., Bartek,J., Baer,R., Lukas,J., and Jackson,S.P. (2007). Human CtIP promotes DNA end resection. Nature 450, 509-514.
30. Shanbhag,N.M., Rafalska-Metcalf,I.U., Balane-Bolivar,C., Janicki,S.M., and Greenberg,R.A. (2010). ATM-dependent chromatin changes silence transcription in cis to DNA double-strand breaks. Cell 141, 970-981.
31. Sheu,J.J., Guan,B., Choi,J.H., Lin,A., Lee,C.H., Hsiao,Y.T., Wang,T.L., Tsai,F.J., and Shih,I. (2010). Rsf-1, a chromatin remodeling protein, induces DNA damage and promotes genomic instability. J. Biol. Chem. 285, 38260-38269.
32. Shih,I., Sheu,J.J., Santillan,A., Nakayama,K., Yen,M.J., Bristow,R.E., Vang,R., Parmigiani,G., Kurman,R.J., Trope,C.G., Davidson,B., and Wang,T.L. (2005). Amplification of a chromatin remodeling gene, Rsf-1/HBXAP, in ovarian carcinoma. Proc. Natl. Acad. Sci. U. S. A 102, 14004-14009.
33. Singh,T.R., Saro,D., Ali,A.M., Zheng,X.F., Du,C.H., Killen,M.W., Sachpatzidis,A., Wahengbam,K., Pierce,A.J., Xiong,Y., Sung,P., and Meetei,A.R. (2010). MHF1-MHF2, a histone-fold-containing protein complex, participates in the Fanconi anemia pathway via FANCM. Mol. Cell 37, 879-886.
34. Smeenk,G. and van Attikum,H. (2013). The chromatin response to DNA breaks: leaving a mark on genome integrity. Annu. Rev. Biochem. 82, 55-80.
35. Smeenk,G., Wiegant,W.W., Marteijn,J.A., Luijsterburg,M.S., Sroczynski,N., Costelloe,T., Romeijn,R.J., Pastink,A., Mailand,N., Vermeulen,W., and van Attikum,H. (2013). Poly(ADP-ribosyl)ation links the chromatin remodeler SMARCA5/SNF2H to RNF168-dependent DNA damage signaling. J. Cell Sci. 126, 889-903.
36. Smeenk,G., Wiegant,W.W., Vrolijk,H., Solari,A.P., Pastink,A., and van Attikum,H. (2010). The NuRD chromatin-remodeling complex regulates signaling and repair of DNA damage. J. Cell Biol. 190, 741-749.
37. Soutoglou,E. and Misteli,T. (2008). Activation of the cellular DNA damage response in the absence of DNA lesions. Science 320, 1507-1510.
38. Stewart,G.S., Panier,S., Townsend,K., Al-Hakim,A.K., Kolas,N.K., Miller,E.S., Nakada,S., Ylanko,J., Olivarius,S., Mendez,M., Oldreive,C., Wildenhain,J., Tagliaferro,A., Pelletier,L., Taubenheim,N., Durandy,A., Byrd,P.J., Stankovic,T., Taylor,A.M., and Durocher,D. (2009). The RIDDLE syndrome protein mediates a ubiquitin-dependent signaling cascade at sites of DNA damage. Cell 136, 420-434.
39. Tao,Y., Jin,C., Li,X., Qi,S., Chu,L., Niu,L., Yao,X., and Teng,M. (2012). The structure of the FANCM-MHF complex reveals physical features for functional assembly. Nat. Commun. 3, 782.
40. Vyas,R., Kumar,R., Clermont,F., Helfricht,A., Kalev,P., Sotiropoulou,P., Hendriks,I.A., Radaelli,E., Hochepied,T., Blanpain,C., Sablina,A., van,A.H., Olsen,J.V., Jochemsen,A.G., Vertegaal,A.C., and Marine,J.C. (2013). RNF4 is required for DNA double-strand break repair in vivo. Cell Death. Differ. 20, 490-502.
41. Wang,B. and Elledge,S.J. (2007). Ubc13/Rnf8 ubiquitin ligases control foci formation of the Rap80/Abraxas/Brca1/Brcc36 complex in response to DNA damage. Proc. Natl. Acad. Sci. U. S. A 104, 20759-20763.
42. Wang,G.G., Allis,C.D., and Chi,P. (2007). Chromatin remodeling and cancer, Part II: ATP-dependent chromatin remodeling. Trends Mol. Med. 13, 373-380.
43. Weinstock,D.M., Nakanishi,K., Helgadottir,H.R., and Jasin,M. (2006). Assaying double-strand break repair pathway choice in mammalian cells using a targeted endonuclease or the RAG recombinase. Methods Enzymol. 409, 524-540.
44. Yan,Z., Delannoy,M., Ling,C., Daee,D., Osman,F., Muniandy,P.A., Shen,X., Oostra,A.B., Du,H., Steltenpool,J., Lin,T., Schuster,B., Decaillet,C., Stasiak,A., Stasiak,A.Z., Stone,S., Hoatlin,M.E., Schindler,D., Woodcock,C.L., Joenje,H., Sen,R., de Winter,J.P., Li,L., Seidman,M.M., Whitby,M.C., Myung,K., Constantinou,A., and Wang,W. (2010). A histone-fold complex and FANCM form a conserved DNA-remodeling complex to maintain genome stability. Mol. Cell 37, 865-878.
45. Zeitlin,S.G., Baker,N.M., Chapados,B.R., Soutoglou,E., Wang,J.Y., Berns,M.W., and Cleveland,D.W. (2009). Double-strand DNA breaks recruit the centromeric histone CENP-A. Proc. Natl. Acad. Sci. U. S. A 106, 15762-15767.

SUPPLEMENTAL INFORMATION

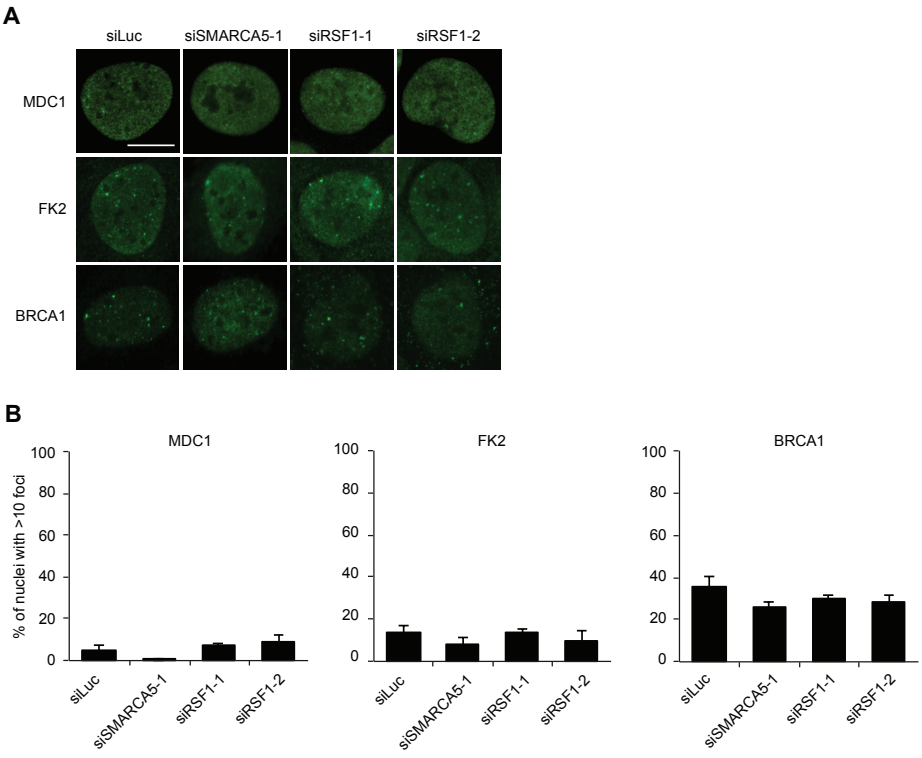

Figure S1. Analysis of spontaneous MDC1, conjugated ubiquitin and BRCA1 in unchallenged SMARCA5 and RSF1 knockdown cells. (A) U2OS cells were transfected with the indicated siRNAs. After 48 h cells were exposed to 2Gy IR or left untreated, and 1 h later immunostained for MDC1, conjugated ubiquitin (FK2) or BRCA1. Representative images of untreated cells showing spontaneously formed foci are presented. Those of IR-exposed cells are presented in Fig. 2 (Fig. 2, c). Scale bar, 10 µm. (B) Quantitative representation of foci formation in A. The average of the percentage of cells with more than 10 foci +/- s.e.m. is presented. More than 120 nuclei were scored per sample in 2-3 independent experiments.

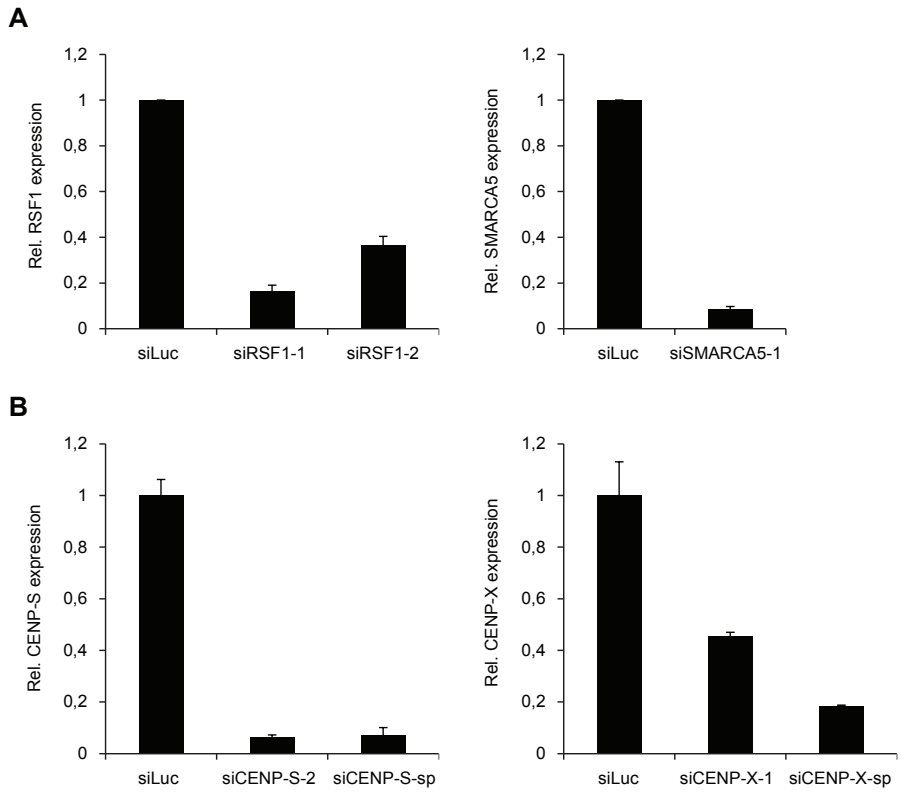

Figure S2. Expression analysis of RSF1, SMARCA5, CENP-S and CENP-X in different knockdown cell lines. U2OS cells were transfected with the indicated siRNAs and 48 h later subjected to RNA extraction. cDNA was synthesized from total RNA samples followed by qPCR to determine the expression levels of RSF1 and SMARCA5 (A), or CENP-S and CENP-X (B) relative to the GAPDH and GUSB reference genes.

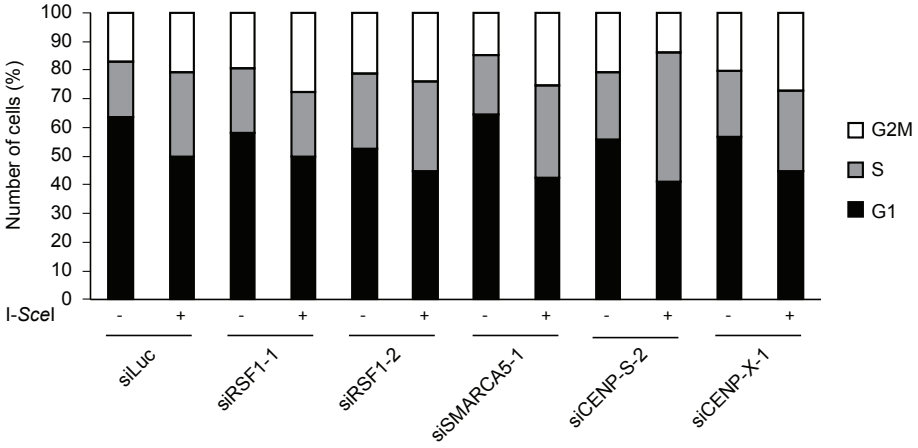

Figure S3. Knockdown of RSF1, SMARCA5, CENP-S or CENP-X does not affect cell cycle progression. HEK293T cells containing the DR-GFP reporter system were transfected with the indicated siRNAs. After 48 h cells were transfected with an ISceI expression vector (pCBASce). 24 h later cells were stained with propidium iodide and subjected to flow cytometry analysis. The percentage of cells in G1 (black bar), S (grey bar) and G2/M (white bar) phase is represented.

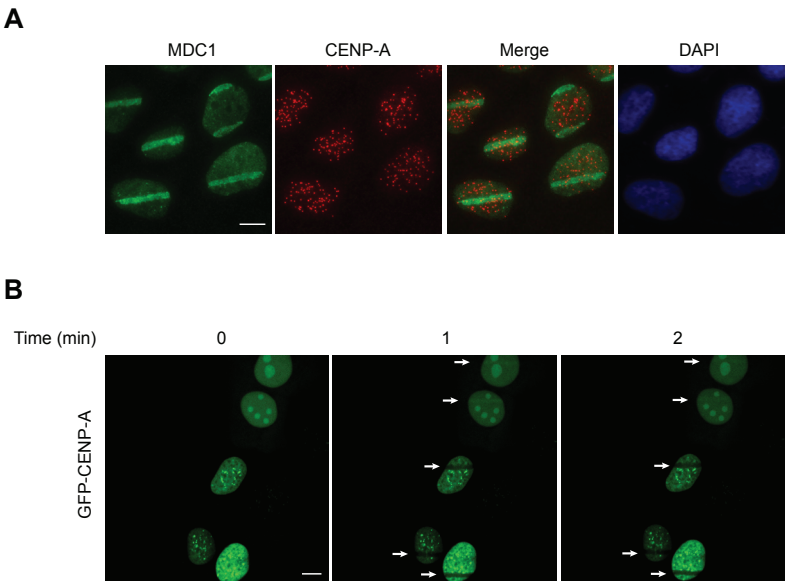

Figure S4. Analysis of CENP-A and GFP-CENP-A recruitment to sites of DNA damage. (A) U2OS cells were subjected to multiphoton laser irradiation and immunostained for MDC1 and endogenous CENP-A at 10 min after irradiation. Scale bar, 10 µm. (B) As in A, except that U2OS cells stably expressing GFP-CENP-A were used. Representative images are shown for the indicated time-points. Arrows indicate micro-irradiated areas.

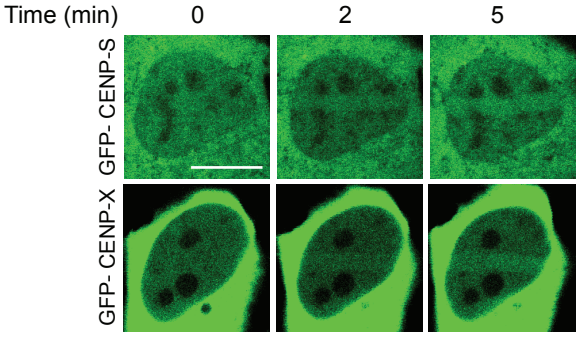

Figure S5. GFP-CENP-S and CENP-X accumulate at damaged chromatin. (A) U2OS cells transiently expressing GFP-CENP-S or GFP-CENP-X were irradiated using a multiphoton laser and subjected to real-time recording of protein assembly at the damaged area. Images show recruitment of GFP-CENP-S and GFP-CENP-X at the indicated time-points. Scale bar, 10 µm.

>

Figure S6. Recruitment of SMARCA5 and RSF1 to sites of DNA damage is mutually independent. (A) U2OS cells stably expressing SMARCA5-GFP or GFPRSF1 were laser-irradiated and subjected to real-time recording of protein assembly at the damaged area. Scale bars, 10 µm. (B) Quantitative representation of results in A. Relative Fluorescence Units (RFU) are plotted on a time scale. Graphs represent the mean +/- s.e.m. of at least 25 individual cells from 2 independent experiments. (C) As in A, except that U2OS cells stably expressing SMARCA5-GFP were used and transfected with siRNAs against RSF1. (D) As in B, except that cells from C were analyzed. (E) As in A, except that U2OS cells stably expressing GFP-RSF1 were used and transfected with siRNAs against SMARCA5. (F) As in B, except that cells from E were analyzed. (G) RSF1 and SMARCA5 levels were monitored by western blot analysis using whole cell extracts of cells in C and F. Tubulin is a loading control.

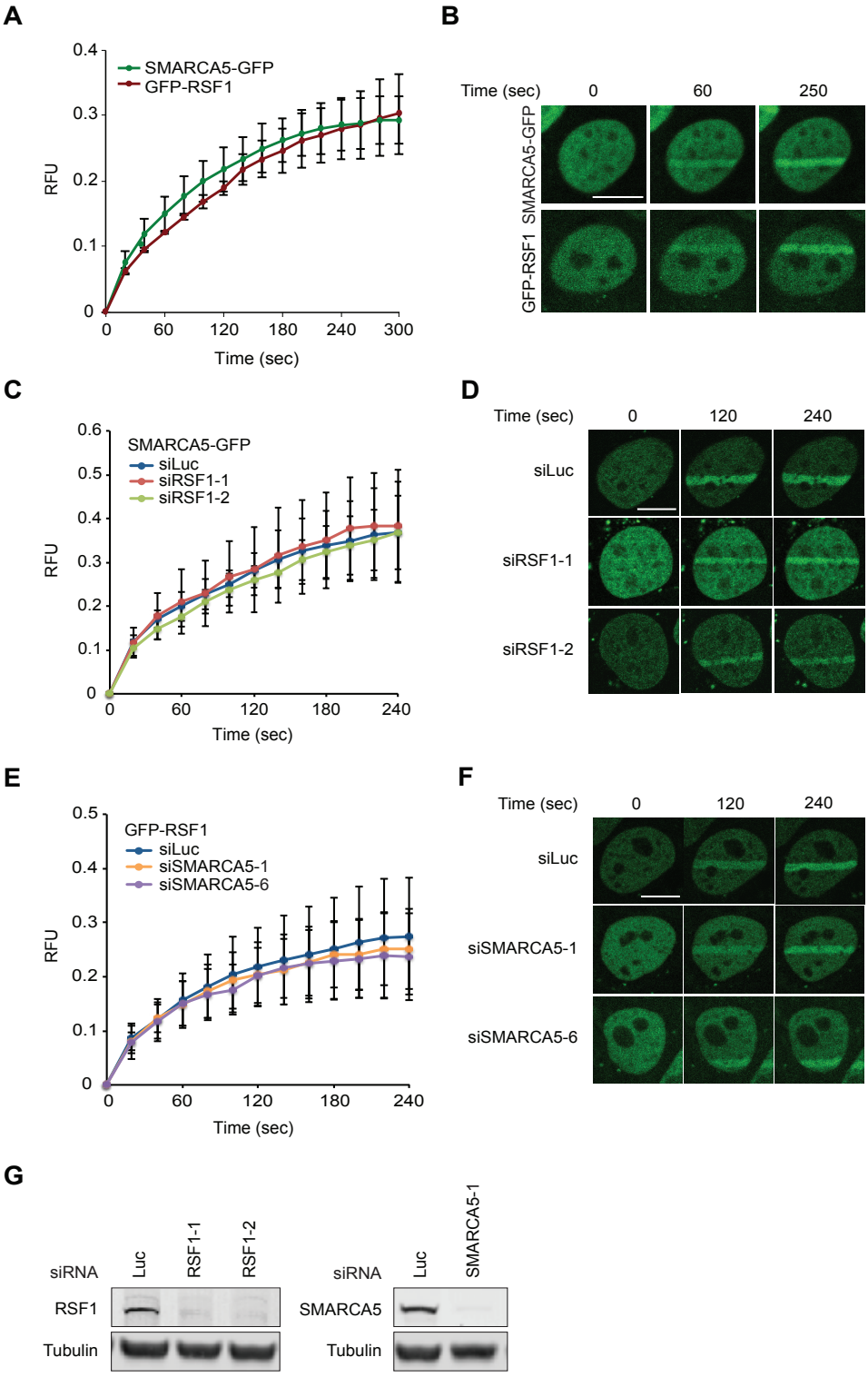
A
SMARCA5-GFP
GFP-RSF1
RFU
Time (sec)
B
Time (sec)
0
60
250
SMARCA5-GFP
GFP-RSF1
C
SMARCA5-GFP
siLuc
siRSF1-1
siRSF1-2
RFU
Time (sec)
D
Time (sec)
0
120
240
siLuc
siRSF1-1
siRSF1-2
E
GFP-RSF1
siLuc
siSMARCA5-1
siSMARCA5-6
RFU
Time (sec)
F
Time (sec)
0
120
240
siLuc
siSMARCA5-1
siSMARCA5-6
G
siRNA
Luc
RSF1-1
RSF1-2
RSF1
Tubulin
siRNA
Luc
SMARCA5-1
SMARCA5
Tubulin

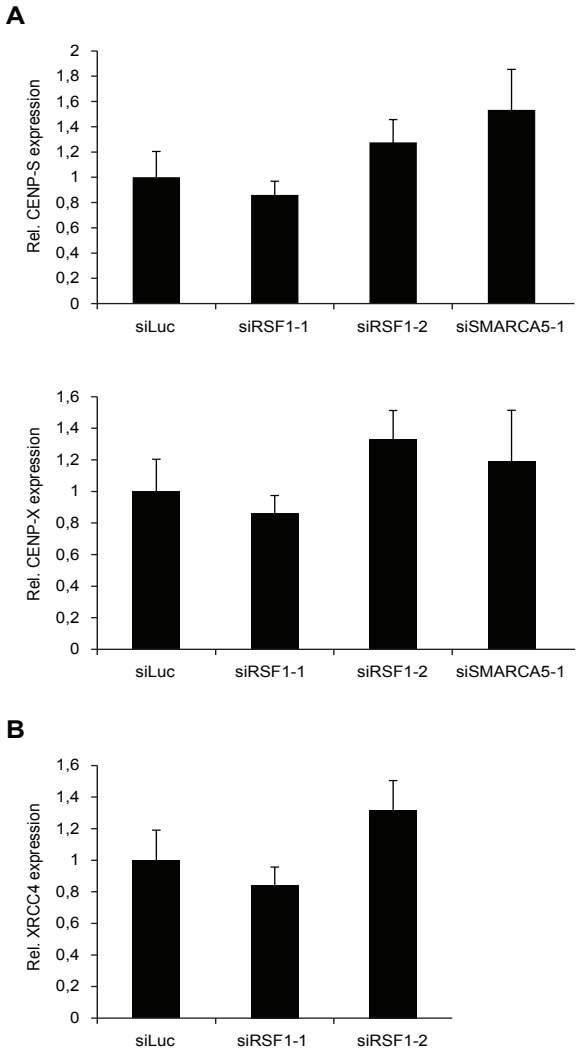

Figure S7. Expression analysis of CENP-S, CENP-X and XRCC4 in RSF1 and SMARCA5 knockdown cells. U2OS cells were transfected with the indicated siRNAs and 48 h later subjected to RNA extraction. cDNA was synthesized from total RNA samples followed by qPCR to determine the expression levels of CENP-S and CENP-X (A), or XRCC4 (B) relative to the GAPDH and GUSB reference genes.

Tabel S1: Primers used for RT-qPCR-based gene expression analysis

Gene	Forward primer (5'>3')	Reverse primer (5'>3')
GAPDH	GAGTCAACGGATTTGGTCGT	TTGATTTTGGAGGGATCTCG
GUSB	CTCATTTGGAATTTTGCCGATT	CCGAGTGAAGATCCCCTTTTTA
RSF1	GCGAAGACTTTCCAGCTCAG	CGAACTGACCGCTTTGATTC
SMARCA5	AAACGAGGACCAAAGCCTTC	TTTTTCTTCCTCGACCATCAG
CENP-S	CTGAAGATGTGAAGCTCTTAGCC	GGCTGCCTTGAATTTTTGC
CENP-X	TGGACTTCTAGGGATCTCAGC	CAAATCCTTCAGGTCCTTCC
XRCC4	AGGAGACAGCGAATGCAAAG	TGTTTTCAGCTGAGATGTGCTC